ORIGINAL PAPER: SOL-GEL AND HYBRID MATERIALS FOR OPTICAL, PHOTONIC AND OPTOELECTRONIC APPLICATIONS

Check for updates

Study on microstructural and electro-optical properties of sol–gel derived pure and Al/Cu-doped ZnO thin films

Fatemeh Dabir[1] · Hamid Esfahani[2] · Fatemeh Bakhtiargonbadi[2] · Zahra Khodadadi[2]

Abstract

In this study, pure and doped ZnO thin films were prepared by sol–gel-based method and their electro-optical properties were investigated. For doping process, 1 at. % Al and Cu was incorporated in ZnO solution separately, and the thin films were prepared by dip coating method. The microstructure and morphology of calcined ZnO, Al-doped ZnO, and Cu-doped ZnO thin films were evaluated and compared by using various techniques X-ray diffraction (XRD), energy dispersive spectroscopy (EDS), and field emission scanning electron microscopy (FESEM). Results showed that nanostructured ZnO thin films with cross-linked nanoparticles (NPs) were formed, and the size of ZnO NPs increased with the Al and Cu doping. It was also found that the substitution and interstitial of Al and Cu dopants caused the instability of ZnO crystal structure and generation of extra point defects. Photoluminescence (PL) properties indicated that the dopants incorporation causes the decline of the PL intensity and the shift of the localized energy states of electrons and holes to lower energy levels. Evaluation of thin films in the UV–Vis range demonstrated that the transparency increased (>94%), and the band gap decreased to 3.08 and 3.06 eV with the incorporation of Al and Cu into ZnO thin films, respectively. The electrical conductivity also improved by Al and Cu doping of ZnO TFs.

Graphical Abstract
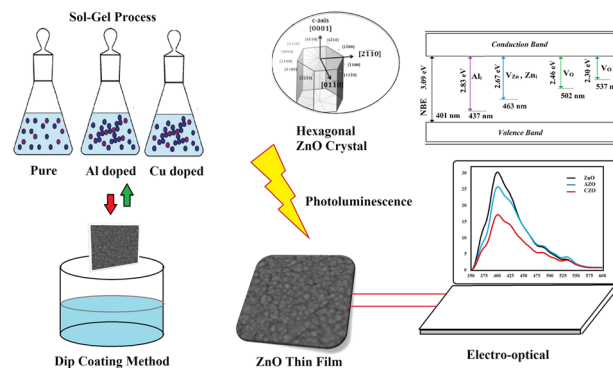
✉ Hamid Esfahani
  h.esfahani@basu.ac.ir

1   Non-Metallic Materials Research Group, Niroo Research Institute
    (NRI), Tehran, Iran

2   Department of Materials Engineering, Bu-Ali Sina University,
    Hamedan 65178-38695, Iran

Highlights

- Nanostructured sol-gel doped ZnO thin films show the promising electro-optical properties.
- Al and Cu dopant could change the parameters of ZnO lattice network.
- Optical band gap reduced by generation of point defects those act as luminescence quenchers.

1 Introduction

The progress of technology has caused the development of the transparent conducting oxides (TCOs) thin films owing to their wide electro-optical applications in sensors, solar cells, transistors, electrophotochemical electrodes, and electrophotocatalysts [1–3]. Zinc oxide (ZnO) has drawn much attention in research and industry fields due to its nontoxicity, simple and low cost production, transparency, and thermal stability [4]. In addition, ZnO presents a wide and direct band gap of about 3.37 eV and large exciton binding energy of 60 meV, those make it a suitable substitute for currently industrial TCOs such as pure SnO_2, F-doped SnO_2 (FTO), and Sn-doped In_2O_3 (ITO) [5, 6].

The cation doping on ZnO lattice has become a primary concern in research because dopants can effectively modify the electro-optical, magnetic, and chemical properties of ZnO-based thin films [7]. By engineering the band gap and electron affinity of ZnO through doping, the new defect chemistry is formed in ZnO lattice, which may enhance the functionality of electro-optical devices [7]. The cations like Al^{3+}, Cu^{2+}, Cu^{+}, Ga^{3+}, In^{+}, Ag^{+}, Mg^{2+}, Mn^{2+}, Ni^{2+}, Co^{2+}, Eu^{3+}, and Tb^{3+} are widely doped into ZnO lattices to improve the electro-optical properties [7, 8].

Not only the morphology of the ZnO thin films is changed by doping, but also the different valences between dopants and Zn^{2+} give rise to the achievement of n or p type semiconductor [4, 9]. Among the mentioned cations above, Al^{3+} and Cu^{2+} are widely used as dopants to achieve the n and p type ZnO semiconductor, respectively, because their substitution is occurred with low energy, high ionization rate, and also higher electron–hole recombination [10]. On the one hand, the high carrier concentration in Al-doped ZnO (AZO), and on the other hand, the intraband transition between Cu_{3d} and Zn_{4s} in the conduction band of Cu-doped ZnO (CZO) provide the AZO and CZO thin films as the high conductive and thermally stable TCOs for a wide range of applications; surface acoustic wave devices, light emitting diodes, gas sensors, lasers, space application, and degradation of pollutants [11–13].

Noteworthy, ZnO thin films can be prepared by various techniques, such as chemical vapor deposition, magnetron sputtering, molecular beam epitaxy, spray pyrolysis, electrospinning, and sol–gel process [14–19]. Among them, sol–gel process is a simple and low cost deposition method in which the chemical composition, stoichiometry, and homogeneity of morphology of ZnO thin films are controllable [1]. The advances in preparation of ZnO thin films by sol–gel technique led to the attempt for more ways of control over morphology, crystallization, and surface area of nanostructured ZnO thin films [6, 20]. The functionality of the ZnO thin films can be modified with regard to the application. Makableh et al. [21] prepared 110 nm thick ZnO films by sol–gel method and they found that the spectral response, power conversion efficiency, and quantum efficiency for antireflection application can be improved by incorporation of GaAs dopants. Sharma et al. [9] could provide Y-doped ZnO thin films by sol–gel process with more donor electrons interesting for heterojunction diodes. In the other work, a clear ferromagnetic behavior in Fe-doped ZnO was reported by Ariyakkani et al. [22].

Based on the literature review, the determination of electro-optical properties of pure and doped ZnO thin films are very important, from both viewpoints of preparation method and microstructure. Although, there are several reports on the electro-optical properties of sol–gel derived ZnO films [23], the rare reports have ascribed how Al and Cu can modify the crystal structure of ZnO and subsequently influence its electro-optical properties. In this study, the AZO and CZO thin films were fabricated through sol–gel process and the microstructure and crystallography of pure and doped ZnO thin films were systematically investigated. Both the electrical and optical properties, band gap, defect chemistry, and photoluminescence (PL) were also studied in respect of the UV–Vis and PL spectra.

2 Materials and methods

2.1 Preparation of thin films

To prepare the pure ZnO and doped ZnO thin films, the following procedure was applied. First, zinc acetate dihydrate $(Zn(CH_3COO)_2 \cdot 2H_2O)$ (Merck 108802) as Zn precursor was dissolved in a mixture of isopropanol (C_3H_8O) (Merck 1009952) as solvent and monoethanolamine (Merck 100845) as stabilizer with a concentration of 0.1 M. To prepare solutions containing Al and Cu, aluminum nitrate nonahydrate $(Al(NO_3)_3 \cdot 9H_2O)$ (Merck 101063) as the Al source and copper nitrate trihydrate $(Cu(NO_3)_2 \cdot 3H_2O)$ (Merck 102753) as the Cu source were also added to the ZnO pre-solution separately with respect to the 1 at. % dopant (see Table 1). In order to achieve homogenous sol,

the prepared solutions were stirred at 60 °C for 2 h. After aging for 24 h at room temperature, the pre-solutions were ready to coat on glass substrates. Prior to the coating, the glass samples ($2.5 \times 2.5 \times 0.1$ cm^3) were cleaned sequentially with DI water, acetone, and ethanol within an ultrasonic bath. Figure 1 presents the fellow diagram for preparing the pure and undoped ZnO thin films. The cleaned substrates were dipped into the prepared solutions and withdrawn by a controlled speed of 1 cm·min^{-1}. The drying process was carried out into an oven at 80 °C for 10 min. The dipping process for all samples was repeated three times. Finally, the obtained films were heat-treated at 400 °C for 1 h. The samples known as ZnO, AZO, and CZO thin films were provided for further investigations.

2.2 Characterization

The structural properties of samples were evaluated by X-ray diffraction (XRD) technique (diffractometer Philips xpert-MPD) using Kα Cu 1.5406 Å radiation. The field emission scanning electron microscopy (FESEM) (T-Scan) equipped with an energy dispersive spectrometer (EDS) was used in order to identify the morphology and composition of thin films. The ImageJ software (1.38× NIH USA) was assigned to analyze the particle size. The electro-optical properties of pure and doped ZnO thin films were studied by the PL (Perkin-Elmer system with $\lambda = 325$ nm and at room temperature). Also UV–Vis spectrophotometer

(Photonix-Ar) was used to investigate the transparency and optical band gap of thin films. The sheet resistance of thin films was identified by four-point probe method. To ensure the reproducibility, all measurements were repeated for three times and the average value was reported.

3 Results and discussion

3.1 Microstructure and composition of thin films

The dip coating process is the beneficial method to fabricate nanostructured thin films from the sol–gel sources. Figure 2 shows the FESEM images of dip-coated ZnO, AZO, and CZO layers calcined at 400 °C. According to this figure, in all samples, spherical nanoparticles (NPs) have been evenly distributed on substrates. It is worth to mention that not only ZnO NPs could be linked in cross point, but also AZO and CZO NPs could obtain the similar arrangement. It was found that the average size of particles forming the ZnO, AZO, and CZO thin films was 6, 22, and 24 nm, respectively. The similar findings were also observed by Yoon et al. [20]. The doping of the Al and Cu elements resulted in an increase in the particle size of the ZnO thin films. It is because that the Al and Cu probably unstabilized the ZnO crystal network and in subsequent it accelerated the grain growth during calcination at 400 °C [24]. In spite of purity of the ZnO thin films, the sol–gel dip coating procedure caused to form nanostructured thin films in which the electro-optical properties would be enhanced [25].

To understand the presence of Al and Cu in the structure of thin films, EDS spectra were provided. Figure 3 displays the EDS spectra of ZnO, AZO, and CZO thin films. In all spectra, the peaks of Si, Mg, and Ca are related to the glass substrates. The existence of Zn and O peaks in all spectra can be an evidence on the formation of ZnO phase on substrates. Also, the peaks of Al and Cu are observed in the EDS spectra of AZO and CZO thin films, which can be

Table 1 The precursor concentration in pure ZnO and incorporated sol–gel

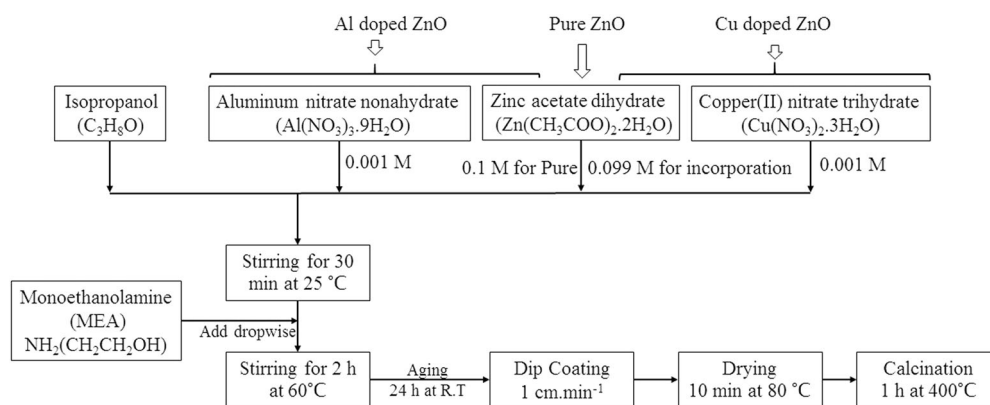| Sol–gel code	Dopant (1 at. %)	Zn(CH$_3$COO)$_2$·2H$_2$O (M)	Al(NO$_3$)$_3$·9H$_2$O (M)	Cu(NO$_3$)$_2$·3H$_2$O (M)
ZnO	–	0.1	0	0
AZO	Al	0.099	0.001	0
CZO	Cu	0.099	0	0.001

Fig. 1 Block diagram shows the preparation of pure and incorporated ZnO TFs by sol–gel method
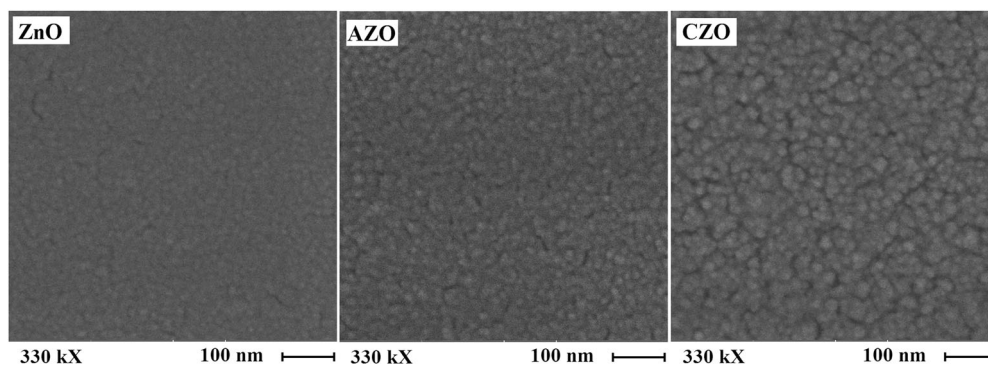
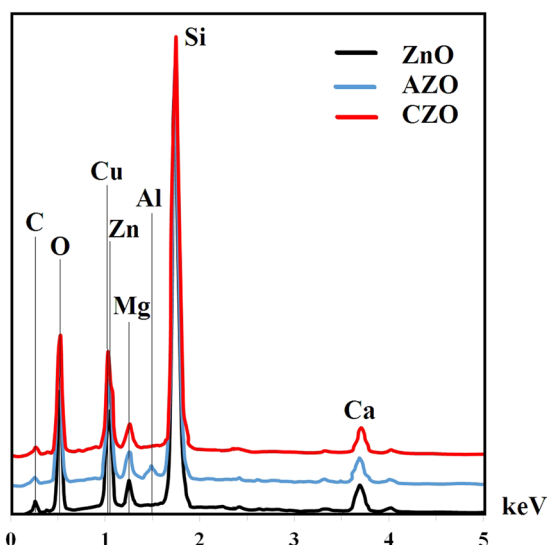Fig. 2 FESEM images of ZnO, AZO, and CZO thin films calcined at 400 °C

Fig. 3 EDS spectra of ZnO, AZO, and CZO thin films calcined at 400 °C

representing the doping of ZnO with Al and Cu, respectively.

As mentioned above, the incorporation of Al and Cu into the ZnO lattice may cause the unstable formation of ZnO crystal network. Hence, the crystallography of pure and doped ZnO thin films were investigated by XRD technique. Figure 4a shows the XRD patterns of ZnO, AZO, and CZO samples. According to the appeared peaks in all patterns, the main formed phase on ZnO, AZO, and CZO is ZnO with hexagonal wurtzite crystal structure (JCPDS; 00-036-1451). It cannot be observed any other peaks in the XRD patterns of ZnO doped with Al (AZO) or Cu (CZO), representing the crystallization of almost pure ZnO without formation of secondary phases such as aluminum and copper oxides. Also, this observation shows that Al^{3+} in the AZO film and Cu^{2+} in the CZO film had not segregation at the grain boundaries of ZnO phase as Al_2O_3 or CuO/Cu_2O. Instead, these dopants may be incorporated into the ZnO lattice.

To further investige the effect of aluminum and copper doping on ZnO microstructure, the XRD patterns of ZnO, AZO, and CZO were re-evaluated carefully in the 2θ range of 30°–40°, which can be seen in Fig. 4b. According to this figure, in the all samples, the sharpest peak is at around 36.3° related to (101) plane of ZnO. Therefore, it may be concluded that the Al and Cu doping had no effect on the preferential crystallization of ZnO phase. However, the doping process has affected the peaks position of (100), (002), and (101) planes, in which these planes diffracted in the lower Bragg angle, meaning the formation of ZnO lattice with longer interplanar distance. It can be also seen that the intensity of (100), (002), and (101) peaks have decreased with aluminum doping, while the intensity of mentioned peaks have increased with copper doping. The average crystallite size of the mentioned planes in ZnO, AZO, and CZO estimated by Scherer equation (Eq. 1) [26] as amounts given in Table 2.

$$D = \frac{0.9\lambda}{\beta \cdot \cos\theta}, \tag{1}$$

where β is the full width at half maximum of the respective peaks. It is clear that the doping of ZnO with Al and Cu decreases its crystallite size, and the crystallite size smaller than 28.3 nm in all samples confirmed the formation of nanostructured ZnO thin films through the sol–gel and post dip coating process.

The lattice parameters of ZnO crystals with hexagonal wurtzite structure (a and c) were estimated by Cohen's equations (Eqs. 2–4) based on the least squares method [27].

$$\Sigma\alpha\sin^2\theta = C\Sigma\alpha^2 + B\Sigma\alpha\gamma + A\Sigma\alpha\delta. \tag{2}$$

$$\Sigma\gamma\sin^2\theta = C\Sigma\alpha\gamma + B\Sigma\gamma^2 + A\Sigma\gamma\delta. \tag{3}$$

$$\Sigma\delta\sin^2\theta = C\Sigma\alpha\delta + B\Sigma\delta\gamma + A\Sigma\delta^2. \tag{4}$$

By assuming $\alpha = (h^2 + hk + k^2)$, $\gamma = l_2$, and $\delta = 10\sin^2 2\theta$, the constants $A = D/10$, $B = \lambda^2/4c^2$, and $C = \lambda^2/3a^2$ can be
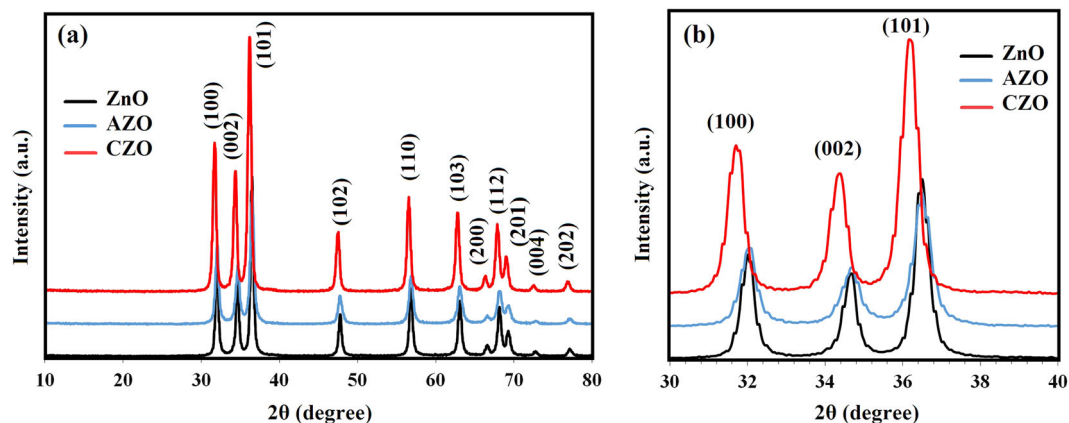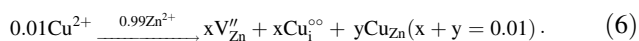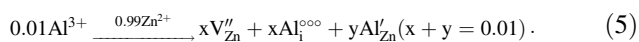
Fig. 4 XRD patterns of ZnO, AZO, and CZO thin films calcined at 400 °C in the range of 10–80° (**a**), and higher magnification in the range of 2θ = 30–40° was carried out to demonstrate the (100), (002), and (101) planes shift with comparison the shift peak the role of Al and Cu dopants on the microstructural ZnO thin film is recognized

Table 2 Lattice parameters of ZnO, AZO, and CZO thin films

Sample code	Crystallite size (nm)			Cell parameters			
	(100)	(002)	(101)	a (Å)	c (Å)	c/a	Unit cell volume (Å^3)
ZnO	28.0	24.1	28.3	3.249	5.195	1.599	47.501
AZO	24.0	21.1	21.2	3.276	5.250	1.603	48.785
CZO	18.6	16.9	21.2	3.264	5.234	1.604	48.287

calculated. The values of a, c, and c/a have been given in Table 2. The unit cell parameters of a and c for ZnO sample obtained 3.249 and 5.195 Å, respectively, which agree with the crystalline specifications given in standard JCPDS 00-036-1451 ($a = 3.2488$ Å, $c = 5.2061$ Å). According to the results, both lattice parameters of a and c for the doped ZnO samples (AZO and CZO) have increased compared with the one of the undoped ZnO sample. Although, the difference in ionic radii between Zn^{2+} (0.074 nm) and dopants of Al^{3+} (0.054 nm) and Cu^{2+} (0.072 nm) may reduce the ZnO lattice parameters due to the substitution of dopants in Zn site [28, 29], it has been demonstrated that the dopants can occupy an interstitial space particularly in low amounts of dopants. Hence, the lattice expansion as well as structure instability are observed [30, 31]. The Kröger–Vink notation for incorporation of 1 at. % Al and Cu in ZnO structure can be presented by the following equations:

$$0.01Al^{3+} \xrightarrow{\quad 0.99Zn^{2+} \quad} xV''_{Zn} + xAl_i^{\circ\circ\circ} + yAl'_{Zn}(x + y = 0.01).\quad (5)$$

$$0.01Cu^{2+} \xrightarrow{\quad 0.99Zn^{2+} \quad} xV''_{Zn} + xCu_i^{\circ\circ} + yCu_{Zn}(x + y = 0.01).\quad (6)$$

In accordance with these equations, by doping 1 at. % Al and Cu into the ZnO structure, extrinsic point defects such as Aluminum and copper interstitials (Al$_i$ and Cu$_i$), zinc vacancies (V_{Zn}), as well as Aluminum and copper substitution (Al$_{Zn}$ and Cu$_{Zn}$) are generated. It should be stated that at higher doping level, dopants segregation may happen at the host grain boundaries and affect the grain growth [32]. The results indicated that the Al and Cu doping of ZnO caused an increase in the preferential growth of c-axis according to the obtained c/a value. The lowest surface energy density of (002) plane is the main reason for the preferential orientation along the c-axis [28] Moreover, a decrease in the crystallite size of (002) plane suggesting the better optical contribution and epitaxial growth [33].

3.2 PL properties of thin films

With doping process, several point defects form into the ZnO host lattice [12, 30]. The defects have a remarkable influence on the electro-optical properties of ZnO thin films. In order to study the effect of Al and Cu dopants on the defects chemistry into the ZnO lattice, the PL spectra for ZnO, AZO, and CZO thin films were provided as shown in Fig. 5 in the range of wavelength of 350–600 nm. The PL phenomenon is influenced by various parameters of excitation energy, size and shape of grains, and impurities [34]. As the grain size of ZnO thin films increased by incorporation of Al and Cu, the intensity of PL peak decreased proportionally, which is due to the decrease in surface area [35]. The emissions in ZnO PL spectrum have two regions, one in the UV region corresponding with excitonic recombination and near band edge (NBE) emissions, and other in the visible region relevant to the structural defects including oxygen vacancies (V_O) and deep level emissions such as zinc vacancies (V_{Zn}), oxygen interstitials (O$_i$), and zinc interstitials (Zn$_i$) [36]. The point defects issued by Al and Cu dopants substituting Zn sites (Al$_{Zn}$, Cu$_{Zn}$) or arised from Al and Cu interstitial sites (Al$_i$, Cu$_i$) also attributed to the visible region. Although the results showed that with the incorporation of Al and Cu, the NBE sharp emission
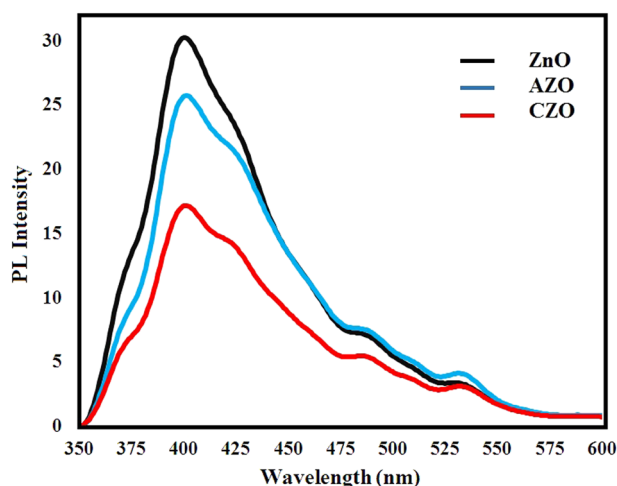
Fig. 5 PL spectra of ZnO, AZO, and CZO thin films

intensity at around 400 nm was reduced, and the more peaks regard to the point defects were turned up in the visible region. The reduction in the intensity of NBE sharp emission is because of the less recombination of free excitons between valence and conduction bands in AZO and CZO thin films [37]. The PL emissions of semiconductor materials occur because of the recombination of the charge carriers stimulated by incident photons. The lower intensity of PL emissions is in accordance with the lower rate of exciton recombination and higher photocatalytic activity of semiconductor photocatalysts [38, 39]. Therefore, it can be elucidated that the incorporation of Al^{3+} and Cu^{2+} into the ZnO lattice reduced the rate of electron–hole recombination and might increase the photocatalytic activity. It should be mentioned that the higher intensity of NBE emission peak compared with the one of green emission peak in the PL spectra of all samples is indicative of high crystallinity and low structural defects of prepared ZnO thin films, which is in good consistency with the XRD findings. Furthermore, regarding the empirical discoveries, the relative intensity of purple to green emissions can be also used as a criterion to evaluate the content of structural defects into the ZnO lattice; higher relative intensity means the lower structural defects density into the ZnO lattice [40]. Hence it can be deduced that the structural defects formed in the doped thin films (AZO and CZO) have higher density comparing the pure ZnO thin films.

In addition to the emission intensity, the wavelength in which a defect emitted has significant role in defects chemistry. For this matter, all PL spectra were deconvoluted to understand the influence of Al and Cu incorruption on optical properties of ZnO thin films. According to the deconvoluted spectra of ZnO, AZO, and CZO thin films presented in Fig. 6a, b, the number of curves fitted on the PL spectrum increased. The results showed that the green

emission issued by a hole recombination with an ionized oxygen vacancy shifted to lower energy levels in the AZO and CZO thin films [41]. The schematic energy band diagrams illustrating the point defect layout in pure and doped ZnO thin films were presented in Fig. 6d–f. It is worth to mention that another green emission was found around 491–502 nm in the AZO and CZO spectra that cannot be observed in the pure ZnO spectrum, it is because of the electrons adjusted to the conduction band and holes trapped at V_O [42]. A violet emission located at around 425 nm that is caused by transitions from the conduction band to V_{Zn} was reduced to the lower energy level in the AZO and CZO spectra, based on the role of aluminum interstitials (Al_i) and complex defect [Cu_{Zn}–Zn_i] in the AZO and CZO thin films, respectively [43]. In addition, Al^{3+} and Cu^{2+} incorporation into the ZnO structure accelerated the electrons transition from the Zn_i to the valence band [44]. It was also found that transition between V_{Zn} acceptor and Zn_i donor in blue to bluish-green region was facilitated at 2.67 and 2.66 eV by presence of Al^{3+} and Cu^{2+} in the ZnO structure, respectively [45, 46].

Since the emission at NBE is created by free exciton recombination, its energy level can be considered as a criterion to evaluate the optical band gap [47]. According to our findings and with respect to the Burstein–Moss effect [48], the band gap of doped ZnO thin films diminished to 3.09 and 3.08 eV for AZO and CZO thin films, respectively. The efficiency of a semiconductor depends on its band gap value, hence further investigation was performed on the electro-optical properties of doped and pure ZnO thin films in the range of UV irradiation.

3.3 Optical and electrical properties of thin films

The transparency of semiconductor thin films is one of the most important properties for many applications [49]. The absorbance spectrum of all doped and pure ZnO thin films were provided in the UV to visible light range, and then the transmittance percentage was plotted versus the wavelength. Figure 7a shows the transmittance spectra for undoped and doped ZnO thin films in 350–900 nm wavelength range. According to these plots, the average transmittance of ZnO, AZO, and CZO thin films was calculated as values given in Table 3. The transparency of 92.8% represents the high transparent ZnO thin films. The doping process of ZnO structure with Al and Cu not only increased its average transparency, but also its adsorption was drastically eliminated under 400 nm wavelength. It is worth to mention that Verma et al. [7] found that the transparency of sol–gel derived ZnO thin films decreased to 80% with doping of 20 at. % Mg.

The band gap of ZnO, AZO, and CZO thin films was estimated by using Tauc's equation [50]. For this matter, the
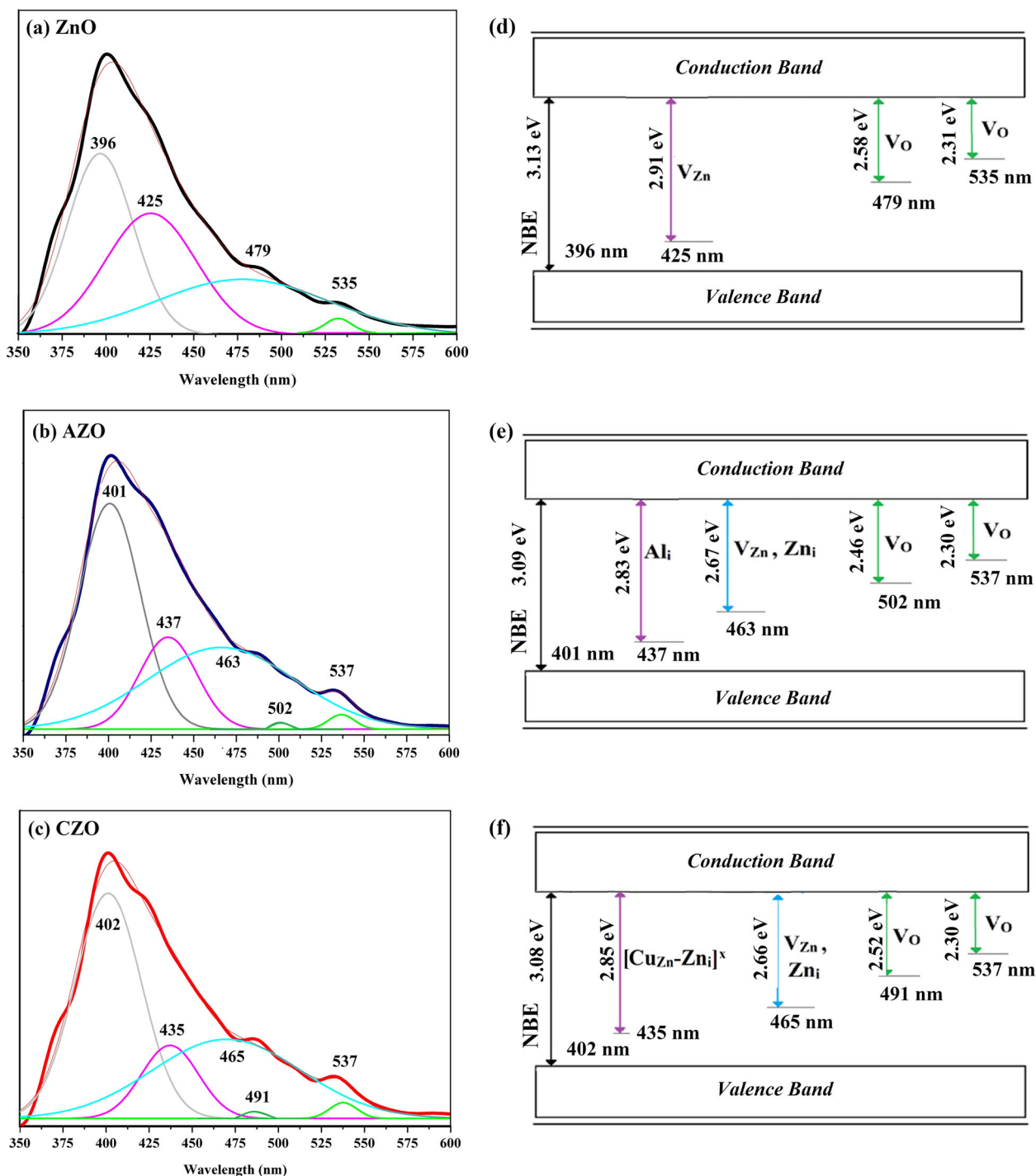
Fig. 6 Deconvolution of PL spectrum for **a** ZnO, **b** AZO, and **c** CZO thin films, and schematic energy band diagram for **d** ZnO, **e** AZO, and **f** CZO thin films

$(\alpha h\nu)^2$ versus $(h\nu)$ curve was extrapolated to find the linear portion intercept based on the following equation:

$$\alpha h\nu = A\left(h\nu - E_g\right)^n, \tag{7}$$

where α is the coefficient of optical absorption and $h\nu$ is the energy of photon. A is a constant, and n is set as 0.5

for direct band gap semiconductors. The optical absorption coefficient depends on the thickness of film (d), and it can be calculated by using the following equation:

$$\alpha = 2.303\frac{\log(\frac{1}{T})}{d}. \tag{8}$$

Fig. 7 a UV transmittance spectra, and **b** absorption spectra $(ah\nu)^2$ versus photon energy ($h\nu$) of ZnO, AZO, and CZO thin films, the higher magnification of intercepts of the linear portion is presented inset of this figure
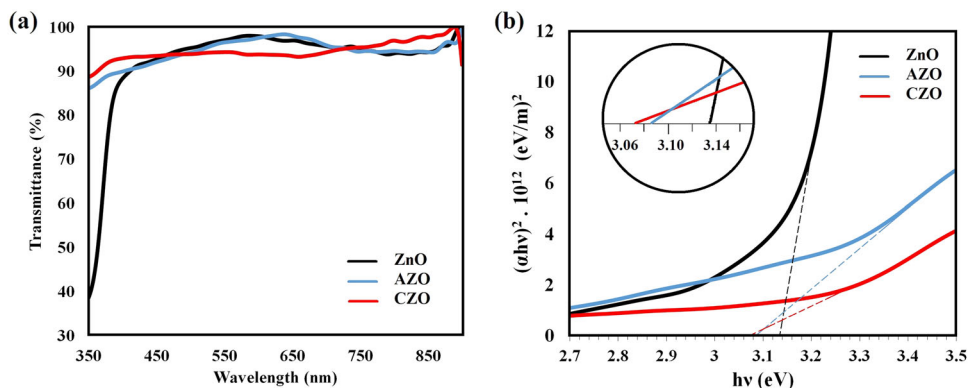

Table 3 Transmittance percentage, band gap value, and sheet resistance of ZnO, AZO, and CZO thin films

Sample code	Transmittance (%)	Band gap (eV)	Sheet resistance (kΩ·sq^{-1})
ZnO	92.8	3.137	8.363 ± 0.28
AZO	94.6	3.082	8.301 ± 0.43
CZO	94.7	3.067	8.239 ± 0.25

As the results given in Table 3, the band gap of ZnO thin films decreased 1.75% and 2.23% with incorporation of 1 at. % Al and Cu in the ZnO structure, respectively. The reduction of rate of electron–hole recombination along with the creation of more point defects caused the decrease in the band gaps of doped ZnO thin films and those ultimately improved the optical properties. Further investigations on electrical properties of prepared thin films were performed by means of sheet resistance measurement. The values given in Table 3 present the reduction of electrical resistance of ZnO thin films with the incorporation of Al and Cu dopants. The high crystalline ZnO structures formed in AZO and CZO thin films mean that there are no secondary phases to destruct the electrical conductivity. In accordance to the results, the Al and Cu dopants could almost decrease the electrical resistance of ZnO thin films due to contributing more free electrons at top surface [51]. In addition, the fewer defects also might be formed at CZO top surface through sol–gel coating and post calcination because defects trap the free charge carriers. The comparison of our findings with others reveals that we could obtain relatively high conductive sol–gel derived ZnO thin films. Hun et al. [52] found sheet resistance of 19.3 kΩ·sq^{-1} for ZnO sol–gel thin films doped with 0.5 mol% Al. Eventually, it can be stated that the higher electrical conductivity and optical transparency of AZO and CZO thin films represent that the Al and Cu elements can be assumed as good candidates for electro-optical modification of ZnO thin films prepared by sol–gel-based method.

4 Conclusion

The effect of Al and Cu dopants on the electro-optical properties of ZnO thin films prepared by sol–gel-based method was investigated. It was observed that the grains size of nanostructured ZnO thin films (6 nm) increased up to 22 and 24 nm with incorporation of Al and Cu, respectively. Also, the lattice structure of ZnO thin films was expanded and the defects such as V_{Zn}, Al_i, Cu_i, Al_{Zn}, and Cu_{Zn} are generated. Meanwhile, the high crystalline and pure hexagonal wurtzite was formed and the size of crystallites decreased in both doping systems. The results clearly depicted that the intensity of PL peaks of Al and CZO thin films has decreased comparing the one of undoped ZnO thin films and this decrease is more in the case of CZO film, which was consistent with the results of grain size. Moreover, the extra point defects were also found in the PL spectra of AZO and CZO thin films such as interstitial aluminum (Al_i) in the AZO and complex defect [Cu_Z–Zn_i] in the CZO thin films. The comparison between NBE bands showed that the dopants could reduce the band gap drastically that it was also confirmed by UV–Vis measurements; 3.137, 3.082, and 3.067 eV in respect of ZnO, AZO, and CZO thin films. The high transparency (>92%) was observed for the pure and doped ZnO thin films in the visible light range. The sheet resistance measurements indicated that Al and Cu could improve the electrical conductivity of ZnO thin films. Overall, it can be deduced that the sol–gel process is a promising method to prepare transparent semiconductor thin films, and particularly the incorporation of Al and Cu dopants can improve the electro-optical properties of ZnO thin films. Based on our findings, there is no significant difference between the two Al and Cu dopants and both enhance electro-optical properties of the ZnO thin films.

Compliance with ethical standards

References

1. Ng ZN, Chan KY, Low CY, Kamaruddin SA, Sahdan MZ (2015) Al and Ga dopedZnO films prepared by a sol–gel spin coating technique. Ceram Int 41:254–258

2. Bouaine A, Bourebia A, Guendouz H, Riane Z (2018) Synthesis and characterization of In doped ZnO thin film as efficient transparent conducting oxide candidate. Optik 166:317–322

3. Viet Vu D, Hai Le D, Xuan Nguyen C, Quang Trinh T (2019) Comparison of structural and electric properties of ZnO-based n-type thin films with different dopants for thermoelectric applications. J Sol-Gel Sci Technol 91:146–153

4. Jafari H, Sadeghzadeh S, Rabbani M, Rahimi R (2018) Effect of Nb on the structural, optical and photocatalytic properties of Aldoped ZnO thin films fabricated by the sol-gel method. Ceram Int 44:20170–20177

5. Prabhu RR, Saritha AC, Shijeesh MR, Jayaraj MK (2017) Fabrication of p-CuO/n-ZnO heterojunction diode via sol-gel spin coating technique. Mater Sci Eng B 220:82–90

6. AlArfaj E, Subahi A (2015) The influence of external magnetic field on the structural and optical properties of nanocrystalline ZnO thin films prepared by dip coating method. Superlattic Micros 86:508–517

7. Verma K, Chaudhary B, Kumar V, Sharma V, Kumar M (2017) Investigation of structural, morphological and optical properties of Mg: ZnO thin films prepared by sol-gel spin coating method. Vacuum 146:524–529

8. Aydın H, Aydın C, Al-Ghamdi AA, Farooq WA, Yakuphanoglu F (2016) Refractive index dispersion properties of Cr-doped ZnO thin films bysol–gel spin coating method Optik 127:1879–1883

9. Sharma SK, Singh SP, Kim DY (2018) Fabrication of the heterojunction diode from Y-doped ZnO thin films on p-Si, substrates by sol-gel method. Solid State Commun 270:124–129

10. Tyona MD, Osuji RU, Asogwa PU, Jambure SB, Ezema FI (2017) Structural modification and band gap tailoring of zinc oxide thin films using copper impurities. J Solid State Electrochem 21 (9):2629–2638

11. Samadi M, Zirak M, Naseri A, Khorashadizade E, Moshfegh AZ (2016) Recent progress on doped ZnO nanostructures for visible-light photocatalysis. Thin Solid Films 605:2–19

12. Sandeep KM, Bhat Shreesha, Serrao FelcyJyothi, Dharmaprakash SM (2018) Effect of 8 MeV electrons irradiation on carrier transport mechanism in ZnO thin films fabricated by sol-gel spin coating technique. Surf Coat Tech 338:96–102

13. Benaboud A, Zaabat M, Aida MS, Boudine B, Benzitouni S, Saidani T (2017) Fe_2O_4/ZnO-nanowires synthesis by dip-coating for Orange II-dye photodegradation. Optik 144:397–405

14. Kaushik VK, Mukherjee C, Ganguli T, Sen PK (2017) Electrical and optical characteristics of aerosol assisted CVD grown ZnO based thin film diode and transistor. J Alloy Compd 696 (5):727–735

15. Mickan M, Helmersson U, Horwat D (2018) Effect of substrate temperature on the deposition of Al-doped ZnO thin films using high power impulse magnetron sputtering. Surf Coat Tech 347 (15):245–251

16. Dai K, Ying MJ, Lian J, Shi YJ, Cao ZS, Song HN, Wei MY, Jiang QF, Zhang C (2019) Optical properties of polar thin films: ZnO (0001) and ZnO (000–1) on sapphire substrate. Opt Mater 94:272–276

17. Amuthan BK, Vinoth S, Karthikeyan V, Roy VAL, Thilakan P (2019) Influence of nitrogen dopant source on the structural, photoluminescence and electrical properties of ZnO thin films deposited by pulsed spray pyrolysis. Ceram Int 45 (18):24324–24330

18. Cetin SS, Uslu I, Aytimur A, Ozcelik S (2012) Characterization of Mg doped ZnO nanocrystallites prepared via electrospinning. Ceram Int 38:4201–4208

19. Istrate AI, Nastase F, Mihalache I, Comanescu F, Gavrila R, Tutunaru O, Romanitan C, Tucureanu V, Nedelcu M, Müller R (2019) Synthesis and characterization of Ca doped ZnO thin films by sol–gel method. J Sol-Gel Sci Technol 92:585

20. Yoon Yeo-Chang, Park Kyoung-Seok, Kim Sam-Dong (2015) Effects of low preheating temperature for ZnO seed layer deposited by sol–gel spin coating on the structural properties of hydrothermal ZnO nanorods. Thin Solid Films 597:125–130

21. Makableh YF, Vasan R, Sarker JC, Nusir AI, Seal S, Manasreh MO (2014) Enhancement of GaAs solar cell performance by using a ZnO sol–gel antireflection coating. Sol Energy Mater Sol Cells 123:178–182

22. Ariyakkani P, Suganya L, Sundaresan B (2017) Investigation of the structural, optical and magnetic properties of Fe doped ZnO thin films coated on glass by sol-gel spin coating method. J Alloy Compd 695:3467–3475

23. Sbeta M, Atilgan A, Atli A, Yildiz A (2018) Influence of the spin acceleration time on the properties of ZnO:Ga thin films deposited by sol–gel method. J Sol-Gel Sci Technol 86:513

24. Islam MR, Rahman M, Farhad SFU, Podder J (2019) Structural, optical and photocatalysis properties of sol–gel deposited Aldoped ZnO thin films. Surf Interfaces 16:120–126

25. Beiraghdar N, Talebian N (2015) Surfactant-assisted ZnO thin films prepared by sol–gel dip coating for applied antibacterial coatings: a comparative study with solvothermal-derived ZnO powders. J Sol-Gel Sci Technol 75:383

26. Patterson A (1939) The Scherrer formula for X-ray particle size determination. Phys Rev 56(10):978–982

27. Corami A, Mignardi S, Ferrini V (2007) Copper and Zinc decontamination from single- and binary-metal solutions using hydroxyapatite. J Hazard Mater 146(1–2):164–170

28. Omri K, Bettaibi A, Khirouni K, El Mir L (2018) The optoelectronic properties and role of Cu concentration on the structural and electrical properties of Cu doped ZnO nanoparticles. Phys B Condens Matter 537:167–175

29. Peng Z, Wu D, Wang W, Tan F, Wang X, Chen J, Qiao X (2017) Effect of metal ion doping on ZnO nanopowders for bacterial inactivation under visible-light irradiation. Powder Technol 315:73–80

30. Osali S, Esfahani H, Karami HR (2018) Effect of Al doping on crystallography and electro-optical properties of ZnO semiconductor thin films prepared by electrospinning. Solid State Sci 83:90–98

31. Osali S, Esfahani H, Dabir F, Tajaslan P (2019) Structural and electro-optical properties of electrospun Cu-Doped ZnO thin films. Solid State Sci 98:106038

32. Chen Z, Yan Q, Zhao Y, Cao M, Wang J, Wang L (2019) The structure and the optical-electrical properties of the ZnO films and the Al:ZnO/N: ZnO homojunction photodiode. J Sol-Gel Sci Technol 91:101

33. Dhamodharan P, Manoharan C, Bououdina M, Venkadachalapathy R, Ramalingam S (2017) Al-doped ZnO thin films grown onto ITO substrates as photoanode in dye sensitized solar cell. Sol Energy 141:127–144

34. Liqiang J, Yichun Q, Baiqi W, Shudan L et al. (2006) Review of photoluminescence performance of nano-sized semiconductor materials and its relationships with photocatalytic activity. Sol Energy Mater Sol Cells 90:1773–1787

35. Baradaran M, Ghodsi FE (2019) Highly efficient visible photocatalytic degradation of MB organic dye by heteromorphic ZnO/

AZO/ZnO nanocatalysts: effect of AZO thickness. J Sol-Gel Sci Technol 92:25–39

36. Hasabeldaim E, Ntwaeaborwa OM, Kroon RE, Swart HC (2019) Structural, optical and photoluminescence properties of Eu doped ZnO thin films prepared by spin coating. J Mol Struct 1192:105–114

37. Chen X, Qingshuang X, Jitao L (2020) Significantly improved photoluminescence properties of ZnO thin films by lithium doping. Ceram Int 46:2309–2316

38. Praveena R, Sameera VS, Mohiddon MdA, Krishna MG (2019) Surface plasmon resonance, photoluminescence and surface enhanced Raman scattering behaviour of Ag/ZnO, ZnO/Ag and ZnO/Ag/ZnO thin films. Phys B 555:118–124

39. Ghosh J, Ghosh R, Giri PK (2018) Tuning the visible photoluminescence in Al doped ZnO thin film and its application in label-free glucose detection. Sens Actuat B Chem 254:681–68

40. Musavi E, Khanlary M, Khakpour Z (2019) Red-orange photoluminescence emission of sol-gel dip-coated prepared ZnO and ZnO:Al nano-crystalline films. J Lumin 216:116696

41. Sajjad M, Ullah I, Khan MI, Khan J, Khan MY, Qureshi MT (2018) Structural and optical properties of pure and copper doped zinc oxide nanoparticles. Results Phys 9:1301–1309

42. Zeng H, Duan G, Li Y, Yang S, Xu X, Cai W (2010) Blue luminescence of ZnO nanoparticles based on non-equilibrium processes, defect origins and emission controls. Adv Funct Mater 20(4):561–572

43. West C, Robbins DJ, Dean PJ, Hayes W (1983) The luminescence of copper in zinc oxide. Phys B+C 116(1–3):492–499

44. Kuriakose S, Satpati B, Mohapatra S (2015) Highly efficient photocatalytic degradation of organic dyes by Cu doped ZnO nanostructures. Phys Chem Chem Phys 17(38):25172–25181

45. Srinatha N, Raghu P, Mahesh HM, Angadi B (2017) Spin-coated Al-doped ZnO thin films for optical applications, Structural, micro-structural, optical and luminescence studies. J Alloy Compd 722:888–895

46. Coman T, Timpu D, Nica V, Vitelaru C, Rambu AP, Stoian G, Olaru M, Ursu C (2017) Sequential PLD in oxygen/argon gas mixture of Al-doped ZnO thin films with improved electrical and optical properties. Appl Surf Sci 418:456–462

47. Salem M, Massoudi I, Akir S, Litaiem Y, Gaidi M, Khirouni K (2017) Photoelectrochemical and opto-electronic properties tuning of ZnO films, effect of Cu doping content. J Alloy Compd 722:313–320

48. Masjedi-Arani M, Salavati-Niasari M (2017) Metal (Mn, Co, Ni and Cu) doped ZnO-Zn2SnO4-SnO2 nanocomposites, Green sol-gel synthesis, characterization and photocatalytic activity. J Mol Liq 248:197–204

49. Alfaro Cruz MR, Ceballos-Sanchez O, Luévano-Hipólito E, Torres-Martínez LM (2018) ZnO thin films deposited by RF magnetron sputtering: effects of the annealing and atmosphere conditions on the photocatalytic hydrogen production. Int J Hydrog Energ 43(22):10301–10310

50. Tauc J, Grigorovici R, Vancu A (1966) Optical properties and electronic structure of amorphous germanium. Phys Status Solidi, B 15(2):627–637

51. Kumar V, Singh RG, Purohit LP, Mehra RM (2011) Structural, transport and optical properties of boron-doped zinc oxide nanocrystalline. J Mater Sci Technol 27(6):481–488

52. Hun JG, Kim SH, Koh JH (2018) Enhanced electrical and optical properties based on stress reduced graded structure of Al-doped ZnO thin films Ceram Int 44:735–741